Annual Status Report-October 1993
Cooperative Agreement No. NCC1 - 169

Name and address of Institution:
North Carolina State University
Mechanical & Aerospace Engineering Department
Raleigh NC 27695-7910
(919) 515 - 5667

Title: **Semi-Span Model Testing in the National Transonic Facility**

Principal Investigator:
Dr. Ndaona Chokani
Research Assistant:
William E. Milholen II

NASA Technical Officer:
Jassim A. Al-Saadi
NASA Langley Research Center
High Reynolds Number Aerodynamics Branch
AAD MS 267
(804) 864 - 5164

Introduction

Over the past several years, transport designers have expressed a renewed interest in semi-span model testing, particularly for the design and optimization of high-lift systems. Figure 1 shows a schematic of a 2-D high-lift system. This particular geometry consists of three elements: a leading edge slat, a main element, and a trailing edge flap. Reference 1 gives a detailed descreption of the flow around 2-D multi-element airfoils. As shown in Fig. 1, the wake shed from the leading edge slat travels downstream and subsequently merges with the boundary layer developing on the main element to form a confluent boundary layer. The confluent boundary layer then travels downstream and merges with the boundary layer developing on the flap. The development of confluent boundary layers is highly dependent on the Reynolds number. As the Reynolds number increases, the boundary layers developing on the slat and main element become thinner. As a result, the location where the slat wake and main element boundary layer merge tends to move further aft. Due to such behavior, the variation of maximum lift coefficient with Reynolds number has been seen to be highly non-linear [2]. For this reason, it is necessary to design and test high-lift systems at flight Reynolds numbers.

To meet this challenge, a semi-span testing technique has been proposed for the NASA Langley Research Center's National Transonic Facility (NTF). Semi-span testing has several advantages including (*i*) larger model size, giving increased Reynolds number capability; (*ii*) improved model fidelity, allowing ease of flap and slat positioning which ultimately improves data quality [3,4] ; and (*iii*) reduced construction costs compared with a full-span model. In addition, the increased model size inherently allows for increased model strength, reducing

aeroelastic effects at the high dynamic pressure levels necessary to simulate flight Reynolds numbers.

The Energy Efficient Transport (EET) full-span model [5] has been modified to become the EET semi-span model. The full-span EET model was tested extensively at both NASA Langley Research Center, and NASA Ames Research Center. The available full-span data will be useful in validating the semi-span test strategy in the NTF. In spite of the advantages discussed above, the use of a semi-span model does introduce additional challenges which must be addressed in the testing procedure. To minimize the influence of the sidewall boundary layer on the flow over the semi-span model, the model must be off-set from the sidewall [3]. Figure 2 shows a schematic diagram of the proposed sidewall mount for the semi-span model. The objective is to remove the semi-span model from the sidewall boundary layer by use of a stand-off geometry. When this is done however, the symmetry along the centerline of the full-span model is lost when the semi-span model is mounted on the wind tunnel sidewall. In addition, the large semi-span model will impose a significant pressure loading on the sidewall boundary layer, which may cause separation. Even under flow conditions where the sidewall boundary layer remains attached. the sidewall boundary layer may adversely effect the flow over the semi-span model [6]. Also, the increased model size and sidewall mounting requires a modified wall correction strategy [7]. With these issues in mind, the semi-span model has been well instrumented with surface pressure taps to obtain data on the expected complex flow field in the near wall region.

This status report summarizes the progress to date on developing the semi-span geometry definition suitable for generating structured grids for the computational research. In addition. the progress on evaluating three state-of-the-art Navier-Stokes codes is presented.

Semi-span geometry definition

The definition of the semi-span geometry is needed primarily for developing structured grids for the computational research. In addition, the geometry definition can be used for developing input to the wall correction codes which will be used in the experimental testing. Figure 3 shows the cross-sectional definition of the semi-span model. The wing definition was obtained from tabulated theoretical coordinates [5]. The fuselage cross-sections were obtained directly from model drawings, which were scanned onto a workstation and discretized. These datafiles are stored on the Cray2 (Voyager) supercomputer in the directory: milholen/EET. An ascii datafile, README, describes the available stations and their format.

The cross-sections were input into various CAD packages to generate a surface geometry definition suitable for use with the GRIDGEN grid generation software. Figure 4 shows an oblique view of the resulting surface geometry. including the sidewall stand-off. Several areas on the semi-span model had to be approximated, since insufficient information was provided from the available sources. These regions included the wing-fuselage fillet, and the wing tip. Direct inspection of the semi-span model indicated that the resulting approximations provided an accurate representation of the geometry. In addition, the horizontal tail fairing present on the semi-span model was added to the database for improved fidelity. Finally, several software packages have been utilized to examine the surface slope and curvature distributions, to verify the smoothness of the resulting database.

Computational code evaluation

The complex geometry of the semi-span model, along with the expected highly three-dimensional flow field around the configuration make the flow solver selection even more important. With this in mind, three current state-of-the-art Navier-Stokes solvers are being evaluated to determine which flow solver would be best suited for the proposed research. As discussed above, the semi-span test technique is being implemented in the NTF for the design, testing, and optimization of high-lift systems for transport aircraft. The flow fields of interest have freestream Mach numbers of approximately .20, which is characteristic of take-off or landing conditions. Under such flow conditions, it may seem plausible that the flow around the semi-span model is largely incompressible. This however, is generally not the case. With high-lift devices deployed, particularly in the leading edge region, localized regions of supersonic flow are possible, which may even include shockwaves [1].

With these issues in mind, two of the flow solvers chosen for the evaluation solve the compressible form of the Navier-Stokes equations. These codes were developed at NASA Langley Research Center, and are: TLNS3D [8], and CFL3D [9]. Another logical reason for including compressible flow solvers in the evaluation procedure is the advanced state of compressible flow solvers. Historically, computational fluid dynamics has been motivated by the need to efficiently and accurately obtain solutions for compressible flow problems. As a consequence, solutions of the incompressible Navier-Stokes equations have only recently become efficient. The third code, INS3D [10], recently developed at NASA Ames Research Center solves the incompressible form of the Navier-Stokes equations. All codes have multi-block capability, necessary for complex geometries, and several turbulence modeling options necessary for the highly three-dimensional flows.

At low Mach numbers, it may be expected that the performance of a compressible flow solver will degrade to the point where either the solver becomes inefficient, or accurate solutions may be unobtainable [11]. This inefficiency stems from the fact that the allowable local time step, determined from stability analysis, is inversely proportional to the local speed of sound [12]. For an incompressible flow, the speed of sound is by definition infinite. As the Mach number is lowered for a compressible flow solver, the speed of sound increases, and can become quite large. This effectively reduces the allowable time step, which translates directly into increased run times. Other problems which can occur at low Mach numbers are illustrated with the following example.

Consider the unsteady compressible continuity equation, written in conservative form:

$$\frac{\partial \rho}{\partial t} + \nabla \cdot \left(\rho \vec{V} \right) = 0 \tag{1}$$

In the absence of high lift devices, the flow around a simple wing geometry is nearly incompressible at low Mach numbers. More precisely, the density is nearly constant, and the unsteady term tends to zero throughout the entire computation. This has two direct implications. First, the equation set is not guaranteed to be hyperbolic, and thus the time marching scheme may become inappropriate. Secondly, many codes use this unsteady term to monitor convergence to steady state. If this term is essentially zero, it may be necessary to monitor another term, or a global parameter such as lift coefficient. In addition, if the flow field is essentially incompressible, it is unnecessary to solve the energy equation simultaneoulsy with

the continuity and momenta equations. For this reason, the energy equation can decouple from the solution procedure, introducing oscillations, and degrading the accuracy of the code [13]. This underscores the need to evaluate the performance of the compressible flow codes at low freestream Mach numbers.

For the evaluation procedure, an experimental data set was chosen which had both a simple geometry, and a freestream Mach number similar to that proposed for the EET semi-span test technique. Figure 5 shows a partial view of a C-O grid employed for the first wing geometry. The unswept rectangular wing has an aspect ratio of six, and is constructed of the NACA 0012 airfoil section. In comparison, the full-span EET model has an aspect ratio of 10. The wind tunnel model had a rounded wing tip, which has been modeled in the grid shown in Fig. 5. Reference 14 gives details of the available experimental data. The second wing geometry is the same wing swept aft 30°. This leading edge sweep angle was chosen because it is nearly identical to that of the EET semi-span model. It should be noted that a wing tip extension was added to the swept wing so that the wing tip would be parallel to the approaching freestream.

Figure 6 shows a comparison of the computational results obtained from both compressible flow solvers to experimental data for the following conditions: $M_\infty = .14$, $\alpha = 6.75°$, $Re = 3.3 \times 10^6$, and $\Lambda = 0°$. Both computations agree quite well with the experimental data. At the inboard station, both computational results are nearly identical. At the outboard station the computations show some differences, however, the predicted pressure distributions are still in good agreement with the data. For brevity, other stations across the wing will not be examined, but similar agreement with data was obtained. This overall agreement over the entire wing surface is illustrated by comparing the computed spanwise load distributions to the experimental data, as shown in Fig. 7. Here η represents the non-dimensional semi-span fraction, c_n the sectional normal force coefficient, and C_N the total wing normal force coefficient. Both computations agree quite well with the experimental data.

Figure 8 compares the computed pressure distributions to experimental data at two spanwise locations for the swept wing geometry. The conditions for this case are: $M_\infty = .14$, $\alpha = 6.75°$, $Re = 3.3 \times 10^6$, and $\Lambda = 30°$. At both stations, the computations show good agreement with the data. The leading edge suction peaks have been consistently underpredicted across the wing surface. This may raise concern about the capability of the compressible solvers to predict the flow around swept wings at low Mach numbers. It should be noted however, that the reflection plane used during the wind tunnel experiment was small in comparison to the wing [14]. In fact, for this particular sweep angle, the tip of the wing was well behind the reflection plane. Given this situation, symmetry at the root plane of the wing would be unlikely [15].

These two test cases have shown that both compressible flow solvers are capable of accurately predicting the low speed flow around the 3-D wing geometries. The obtained solutions showed no signs of oscillations, indicating that no obvious numerical difficulties were introduced by the low freestream Mach number.

Due to difficulties with boundary condition implementation, INS3D could not be run for the C-O grid topologies used above. To demonstrate the codes capability, two-dimensional computations were performed for a NACA 4412 airfoil. For comparison, CFL3D was run

in a 2-D mode, with a freestream Mach number of .20. Figure 9 compares both computed solutions to experimental data [16], for the following conditions: $\alpha = 6.40°$, $Re = 1.8 \times 10^6$. Both computations qualitatively agree well with the data. The INS3D solution shows better agreement than the CFL3D solution, which may be due to the artificially high freestream Mach number for the CFL3D solution. However, the INS3D solution time was approximately four times longer than the CFL3D solution. This is attributed to the fact that INS3D does not presently have a multigrid capability.

Future work

INS3D computations

At present, a new version of INS3D has been obtained. The capability of the code to compute 3-D solutions using C-O grid topologies will be evaluated. Once this has been completed, a computational code will be chosen which will be used for the computational research.

Flat plate boundary layer calculations

A flat plate boundary layer code [17] will be used in conjunction with experimentally measured sidewall boundary layer profiles to determine the virtual origin of the sidewall boundary layer. This will provide velocity profiles which will be imposed at the far-field upstream boundary of the computational domain to simulate the sidewall boundary layer. The flate plate computations will also be useful in examining what influence the wind tunnel sidewall temperature has on the development of the sidewall boundary layer. In addition, real gas effects will be examined, to determine how the developement of the sidewall boundary layer is effected.

Semi-span grid generation

The geometry database discussed above is currently being used with GRIDGEN to generate multiblock structured grids for the computational research.

Free-air computations

The first phase of computations for the semi-span model will focus on the prediction of the "free-air" [6] flow field around the model. This will serve two distinct purposes. First, the computations will provide a baseline which will be used to determine what influence the sidewall boundary layer has on the flow field. The free-air computations will be validated by making direct comparison with the available experimental data. Comparisons will be made to the wing pressure distributions and the available force and moment coefficient data. Once validated, the code would be used as a diagnostic tool to examine the details of the solution.

The second purpose of the free-air calculations is to provide detailed information which will not be easily obtainable in the wind tunnel testing. Such detailed information is not presently available for this geometry, and would be quite useful in the upcoming experimental investigation. This data will also provide the researchers an independent method for evaluating the quality of their data, particularly relating to the wall interference and correction strategy.

Viscous sidewall modeling

The viscous sidewall computations are the primary focus of the research project. The goal is to examine in detail, what influence the sidewall boundary layer has on the flow over the semi-span model. This determination will be made by making direct comparison with the free-air computations, and available experimental data. The comparisons will be made on several levels. The most general comparisons will be between force and moment coefficients, and will give an overall assessment of the influence of the sidewall boundary layer. Detailed comparisons between surface pressure distributions, over the entire model, will give insight as to how the flow field has been modified by the presence of the sidewall boundary layer. The finest level of comparison would examine details of the wing and fuselage boundary layers, and how they have been influenced by the sidewall boundary layer.

The predicted behavior of the sidewall boundary layer is of particular interest. Due to the difficulty in obtaining off-surface measurements in the cryogenic environment, little experimental data can be obtained to characterize the behavior of the sidewall boundary layer. In this particular aspect, the computations will give insight into the inherent juncture flow present in semi-span testing. If the predicted characteristics of the sidewall boundary layer are not acceptable, such as the formation of horseshoe vortices, techniques to improve the flow quality can be computationally examined (such as suction, tangential blowing, or vortex generators).

Acknowledgements

This work was supported by Cooperative Agreement NCC1-169 between North Carolina State University and the High Reynolds Number Aerodynamics Branch at NASA Langley Research Center. The authors thank Jassim A. Al-Saadi for many insightful comments regarding the EET geometry. The authors are grateful to Veer N. Vatsa, Sherri Krist, and Stuart Rogers for many helpful discussions regarding the three Navier-Stokes solvers. The authors would also like to thank L. Elwood Putnam for his support of this work.

References

1. Squire, L.C., *"Interactions Between Wakes and Boundary-Layers,"* Progress in Aerospace Science, Vol. 26, pp. 261-288, 1989.

2. Mack, M.D. and McMasters, J.H., *"High Reynolds Number Testing in Support of Transport Airplane Development (Invited Paper),"* AIAA Paper 92-3982, July 1992.

3. Goldhammer, M.I. and Steinle Jr., F.W., *"Design and Validation of Advanced Transonic Wings Using CFD and Very High Reynolds Number Wind Tunnel Testing,"* Proceedings of the 17^{th} International Council of the Aeronautical Sciences, Paper 90-2.6.2, September 1990, pp. 1028-1042.

4. Boersen, S.J., *"Half-Model Testing in NLR High-Speed Wind Tunnel HST, A 1981 Status Report."* NLR TR 82123 U, August 1982.

5. Morgan Jr.,H.L., *"Model Geometry Description and Pressure Distribution Data From Tests of EET High-Lift Research Model Equipped with Full-Span and Part-Span Flaps,"* NASA TM 80048, February 1979.

6. Milholen II, W.E. and Chokani, N., *"Numerical Modeling of Transonic Juncture Flow,"* AIAA Paper 92-4036, July 1992.

7. Garriz, J.A., Newman, P.A., Vatsa, V.N., Haigler, K.J. and Burdges, K.P., *"Evaluation of Transonic Wall Interference Assessment and Corrections for Semi-Span Wing Data,"* AIAA Paper 90-1433, June 1990.

8. Vatsa, V.N. and Wedan, B.W., *"Development of an Efficient Multigrid Code for 3-D Navier-Stokes Equations."* AIAA Paper 89-1791, June 1989.

9. Thomas, J.L., Taylor, S.L. and Anderson, W.K., *"Navier-Stokes Computations of Vortical Flows Over Low Aspect Ratio Wings,"* AIAA Paper 87-0207, January 1987.

10. Rogers, S.E., *"Progress in High-Lift Aerodynamic Calculations,"* AIAA Paper 93-0194. January 1993.

11. Volpe, G., *"Performance of Compressible Flow Codes at Low Mach Numbers,"* AIAA Journal, Vol. 31, January 1993, pp. 49-56.

12. Anderson, D.A. Tannehill, J.C. and Pletcher, R.H., *"Computational Fluid Mechanics and Heat Transfer,"* Hemisphere Publishing Corporation, New York, 1984.

13. Choi, Y.H. and Merkle, C.L., *"The Application of Preconditioning in Viscous Flows,"* Journal of Computational Physics, Vol. 105, April 1993, pp. 207-223.

14. Yip, L.P and Shubert, G.L., *"Pressure Distributions on a 1-by-3 Meter Semispan Wing at Sweep Angles From 0° to 40° in Subsonic Flow,"* NASA TN D-8307, December 1976.

15. Yip, L.P , *Private Communication*, June 1993.

16. Pinkerton, R.M., *"The Variation with Reynolds Number of Pressure Distribution Over an Airfoil Section."* NACA Report 613, July 1937.

17. Anderson, E.C. and Lewis, C.H., *"Laminar or Turbulent Boundary-Layer Flows of Perfect Gases or Reacting Gas Mixtures in Chemical Equilibrium,"* NASA CR-1893, 1971.

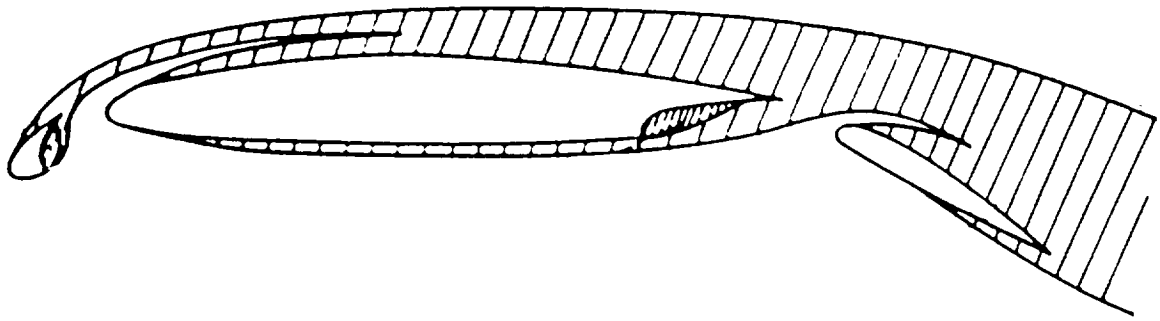

Fig. 1: Schematic of 2-D high lift system.

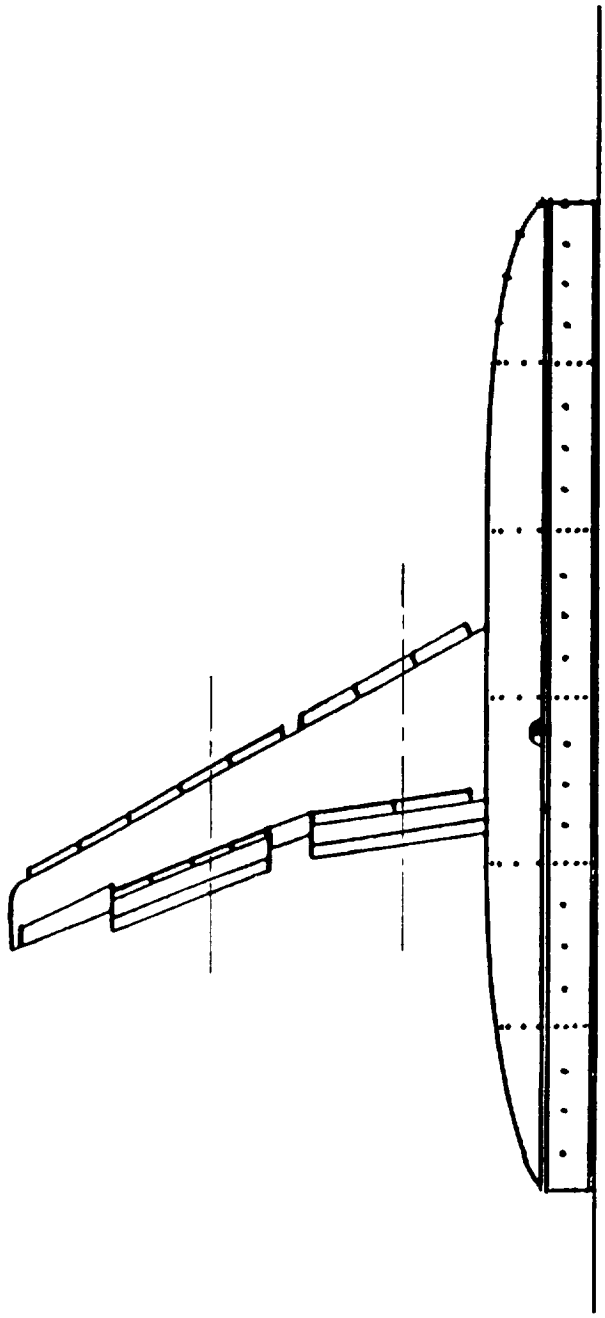

Fig. 2: Schematic of proposed sidewall mounting for EET semi-span model.

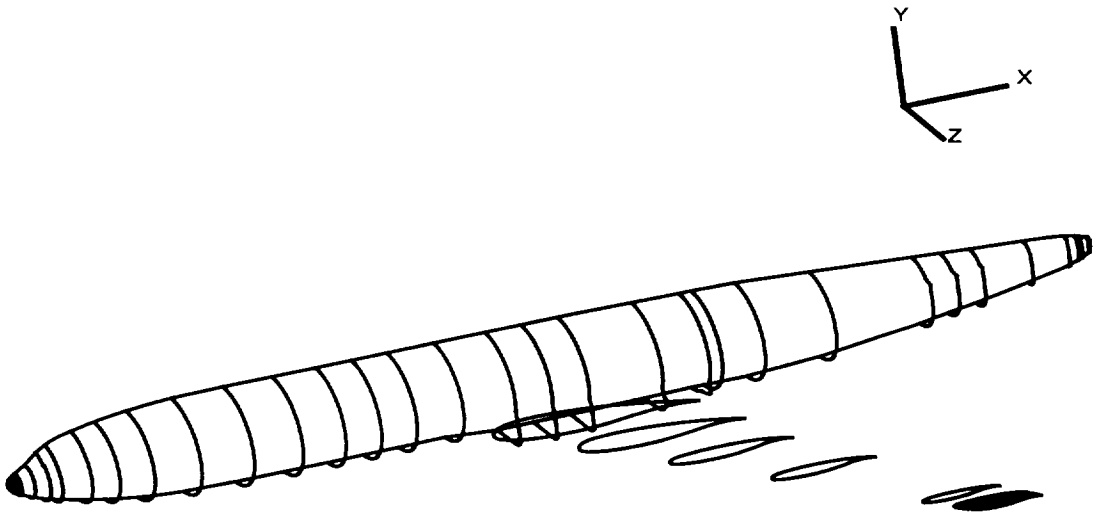

Fig. 3: Cross-sectional geometry definition of EET semi-span model.

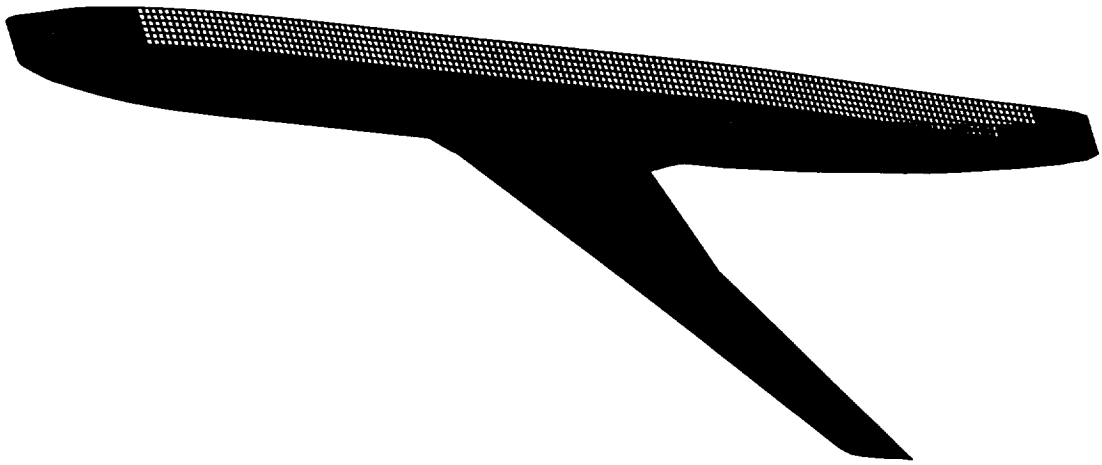

Fig. 4: Surface geometry definition of EET semi-span model.

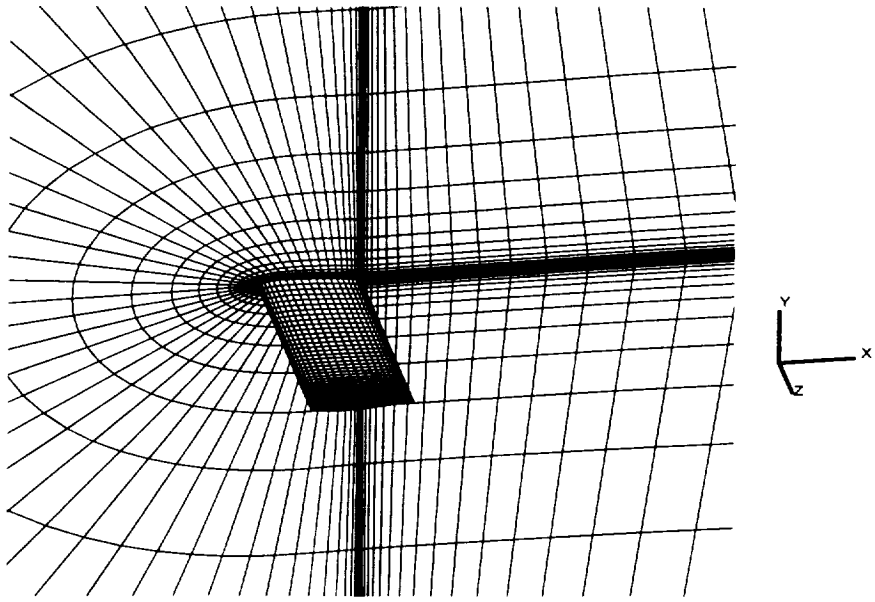

Fig. 5: Partial view of C-O grid topology.

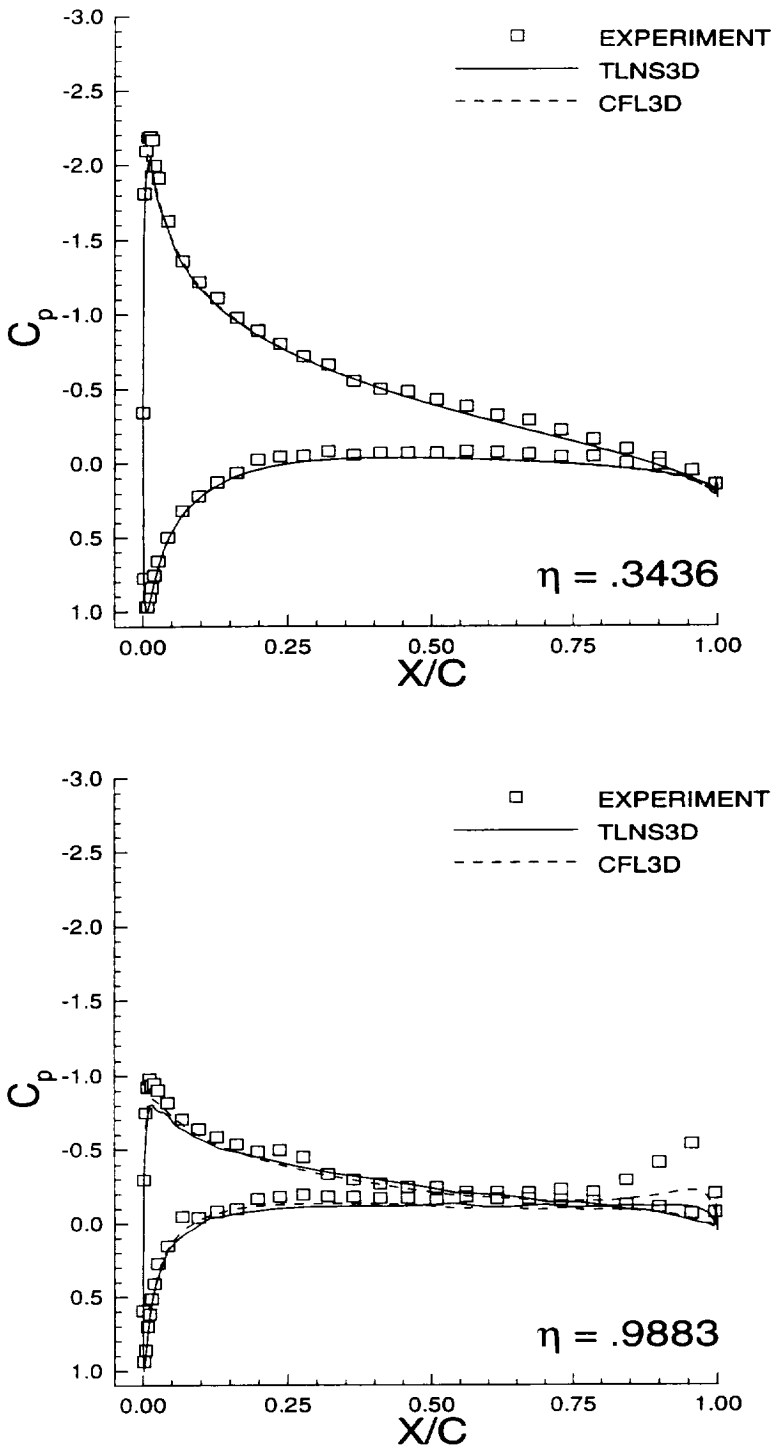

Fig. 6: Comparison of computed pressure distributions with experimental data (M_∞ = .14, α = 6.75°, Re = 3.3 x 10^6, Λ = 0°) .

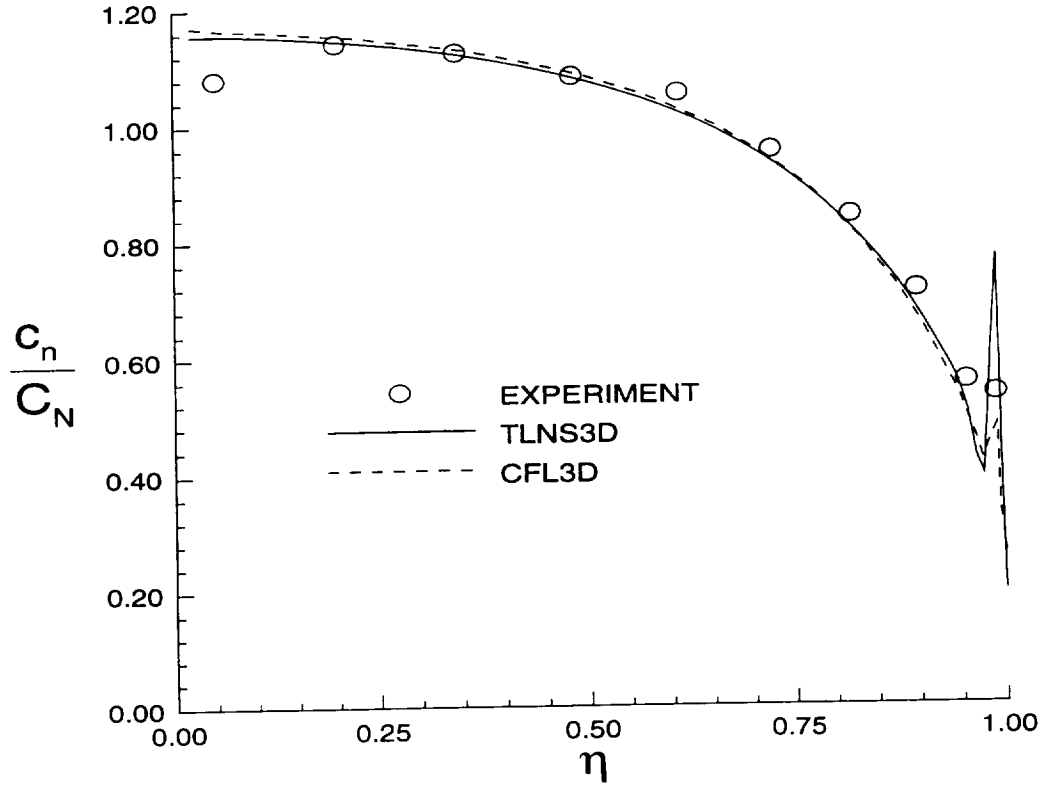

Fig. 7: Comparison of computed spanwise load distributions with experimental data ($M_\infty = .14$, $\alpha = 6.75°$, Re = 3.3 x 10^6, $\Lambda = 0°$) .

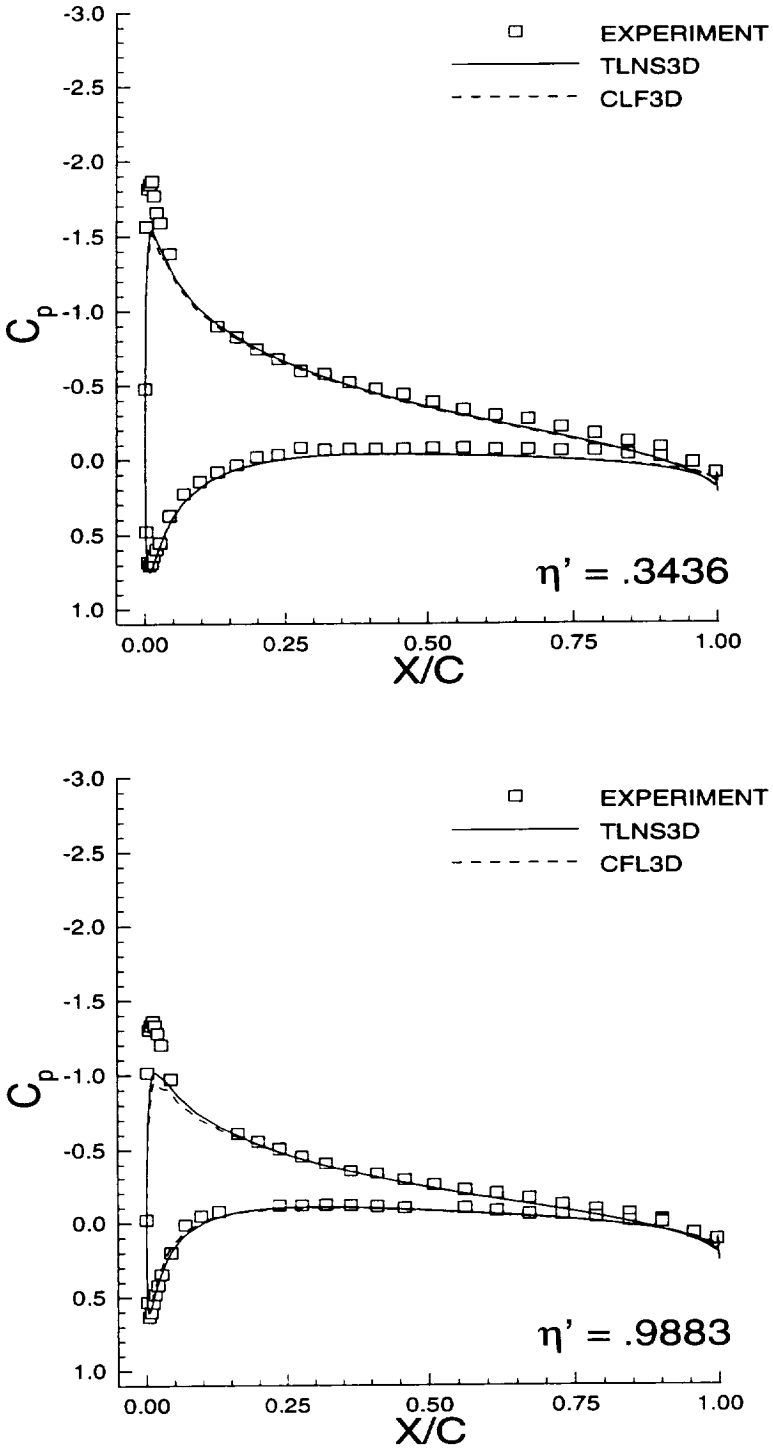

Fig. 8: Comparison of computed pressure distributions with experimental data (M_∞ = .14, α = 6.75°. Re = 3.3 x 10^6, Λ = 30°) .

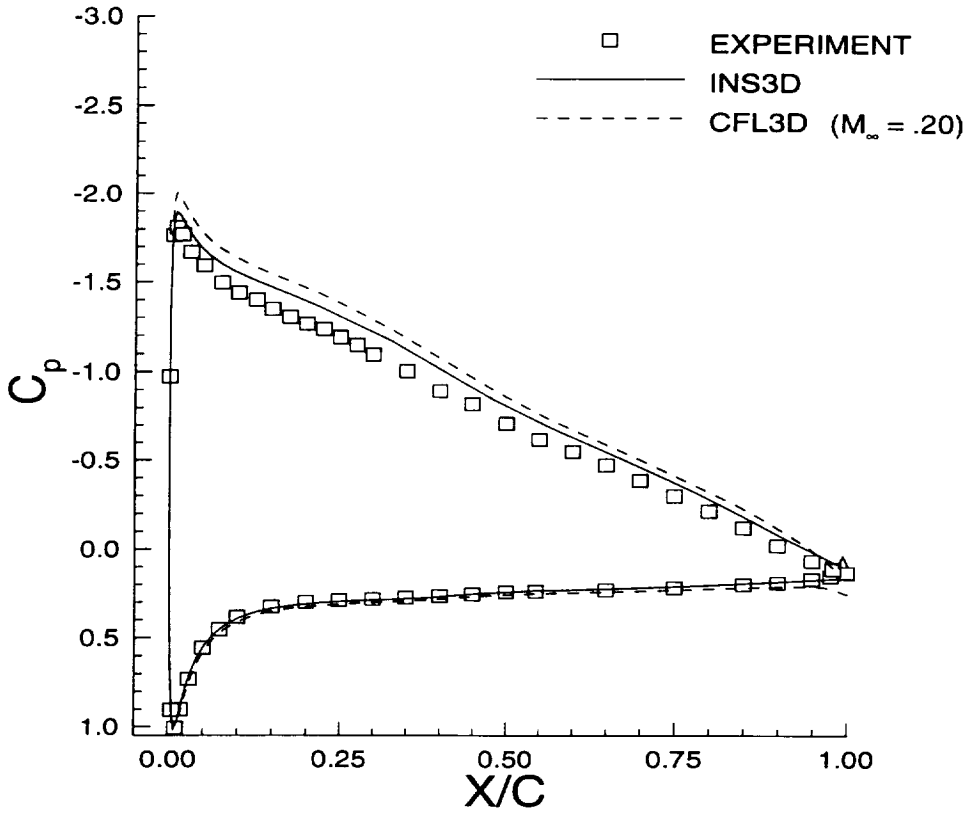

Fig. 9: Comparison of computed pressure distributions with experimental data (NACA 4412, $\alpha = 6.40°$, Re = 1.8 x 10^6) .